Small polaron hopping in spinel manganates

R. Schmidt,* A. Basu, and A. W. Brinkman
Department of Physics, University of Durham, South Road, Durham DH1 3LE, United Kingdom
(Received 19 November 2004; revised manuscript received 26 April 2005; published 1 September 2005)

The temperature dependence of small polaron hopping conduction in ceramic spinel $NiMn_2O_{4+\delta}$ thermistor material has been investigated. We used a theoretical framework based on a random resistor network model to describe small polaron nearest-neighbor hopping (NNH) and variable range hopping (VRH), following the principles of Shklovskii and Efros. We find that in printed thick films and in pressed pellets resistivity is described best by a VRH model of the form $\rho \sim T^{2p} \exp(T_0/T)^p$, whereas in thin $NiMn_2O_{4+\delta}$ films resistivity is better described by NNH, $\rho \sim T \exp(T_0/T)$. Steady state dc resistance vs temperature measurements for $NiMn_2O_{4+\delta}$ thick films, thin films, and pellets have been carried out and the parameters p and T_0 determined. For thick films p was found to be ~ 0.5, indicating VRH with an approximately parabolic distribution of the density of states (DOS) around Fermi level. For pellets p was ~ 0.65, and in thin films ~ 1 indicating NNH. The increase of p was interpreted as an increase of disorder in the system, leading to strong electron localization effects and narrowing Mn^{3+}/Mn^{4+} bandwidth. In thick films and pellets the DOS was determined by a parametrization related to the p value, giving 10^{20}–10^{21} eV^{-1} cm^{-3}. The characteristic temperature T_0 was in the range of 2×10^5 K in thick films, 3×10^4 K in pellets, and 5×10^3 K in thin films.

DOI: 10.1103/PhysRevB.72.115101 PACS number(s): 72.20.Ee, 72.80.−r

I. THE $NiMn_2O_{4+\delta}$ SPINEL SYSTEM

$NiMn_2O_{4+\delta}$ is a strongly correlated system, where the crystal structure and the electrical properties are closely linked.[1] The material has a cubic spinel structure based on an oxygen fcc sublattice, where, in the case of a regular spinel, divalent cations are situated on tetrahedral and trivalent cations on octahedral lattice interstices. $NiMn_2O_{4+\delta}$ is not a regular but intermediate type of spinel where a fraction x of Ni^{2+} cations are displaced from tetrahedral to octahedral interstices. A corresponding proportion $2x$ of trivalent Mn cations disproportionate to Mn^{2+} and Mn^{4+}, and the Mn^{2+} cations move to the tetrahedral sites to compensate Ni^{2+} vacancies.[2] Both an oxygen excess or loss of δ in $NiMn_2O_{4+\delta}$ material can occur depending on the sintering history,[3] and the cation distribution may be described by[4]

$$Ni^{2+}_{1-x}Mn^{2+}_x[Ni^{2+}_x Mn^{3+}_{2-2x-2\delta}Mn^{4+}_{x+2\delta}]O_{4+\delta}, \quad (1)$$

where the square brackets indicate octahedral sites. The oxygen content δ and the inversion parameter x both vary independently with the sintering history, which makes the prediction of the cation distribution difficult. Conduction is based on thermally activated hopping between Mn^{3+} and Mn^{4+} cations on octahedral sites and shows a negative temperature coefficient of resistance (NTCR). Resistivity is sensitive to the cation distribution, i.e., the Mn^{3+}/Mn^{4+} ratio, and hence, for quantitative analysis x and δ need to be determined precisely by titration methods,[3] neutron diffraction,[5] or x-ray photoelectron spectroscopy,[6] which is beyond the scope of this work.

In spinel manganates the basic MnO_6 octahedra are corner shared and the Mn-O-Mn ion alignment angle is far off the 180° angle; thus, double exchange interactions are weak and the compounds exhibit a uniform insulating electronic phase, which is uncoupled from the paramagnetic or antiferromagnetic phase ($T_C \sim 150$ K).[7] The crystal structure of spinels is illustrated in Fig. 1 showing the basic cubic unit cell in full and in eight slices taken in the [100] crystal direction.[8] The octahedral cations in each slice are aligned, whereby the direction of the alignment changes alternating every second layer. The cubic unit cell parameter is $a \sim 8.4$ Å,[9] and the minimum distance between octahedral cations ~ 3.0 Å. Localized Mn^{3+} states are associated with strong electron-phonon coupling and strongly Jahn-Teller distorted $Mn^{3+}O_6$ octahedra. Charge transport is by small polaron hopping, which may be understood from a simple real-space picture, in contrast to classical semiconductors (CS) where charge carriers are delocalized and can be described in momentum space. Localization of donor Mn^{3+} and acceptor Mn^{4+} states arise from the random crystal field fluctuations, the internal degrees of freedom (like orbital angular momentum and spin)[10] and inhomogeneous lattice strain especially near grain boundaries.[11] Such variations broaden localized Mn^{3+} and Mn^{4+} states to form lower and upper Hubbard bands.

Applications of the compound comprise thermistors in temperature sensors and temperature compensating attenuators. Due to activation energies in the infrared regime, application in infrared radiation detection devices for thermal imaging has been considered, too.

II. MOTIVATION OF THIS WORK

In the present study, dc resistance vs temperature (R-T) measurements were carried out for thick films, thin films, and pellets, and the data were analyzed using a data differentiation method to clarify the type of hopping mechanism qualitatively, which had been subject to controversy in the literature. The sensitivity of sample history and cation distribution to the resistivity has led to a great variety of R-T characteristics and an equally diverse set of models,[12–14] the first two being purely empirical. The structure of the density of states (DOS) in $NiMn_2O_{4+\delta}$ was previously investigated

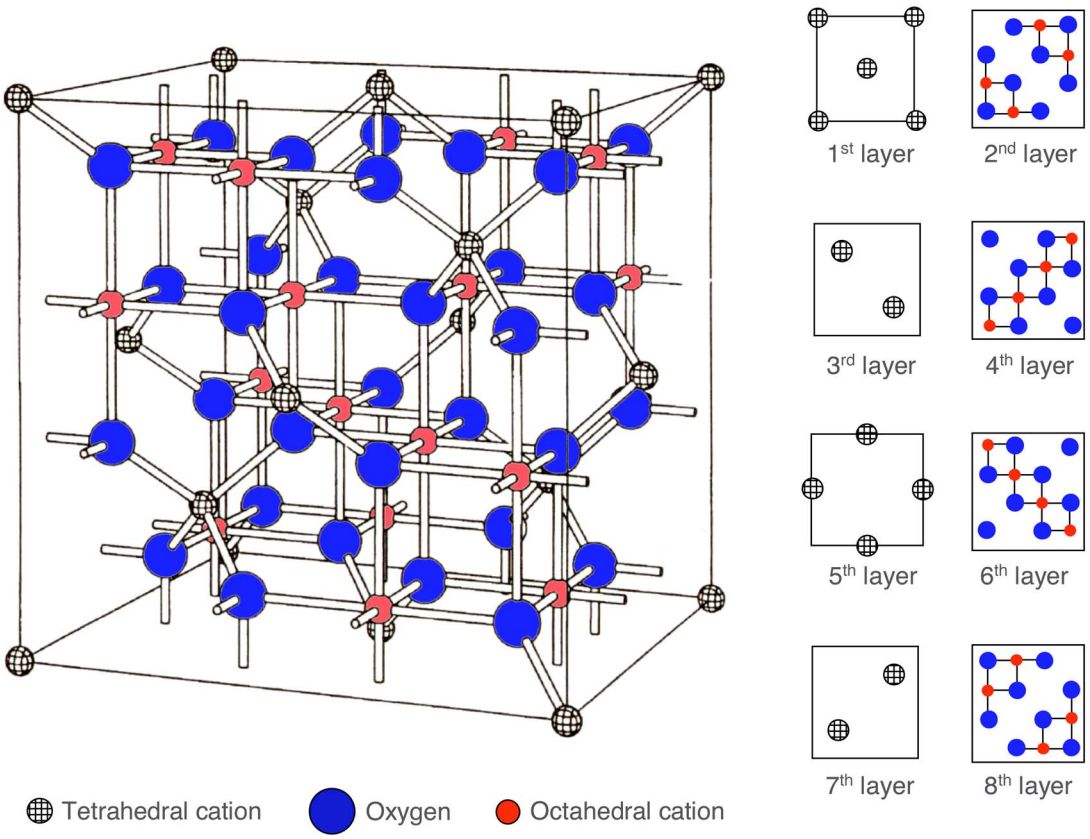

FIG. 1. (Color online) Cubic unit cell in full and in layers taken in the [100] direction.

by combined scanning tunneling microscopy and spectroscopy (STM/STS) and its relation to the electrical transport properties mentioned.[11] This is discussed in more detail here.

The production of layered NTCR thermistor structures is motivated by typical difficulties in bulk material applications, such as poor stability and reproducibility due to incomplete intergranular contact. Furthermore, recent applications of these materials in microwave or LTCC microelectronics make thick-film production interesting,[15,16] whereas thin films are needed in infrared radiation detection devices. As described in previous publications, screen-printing,[17] electron beam evaporation (EBE)[18] and rf magnetron sputtering processes[19] have been developed for thick and thin film NTCR thermistor devices. A high surface density, especially for evaporated and sputtered films was reported,[20] which can minimize the effects of the surrounding ambient such as changes in humidity or variations in oxygen partial pressure.

III. POLARON HOPPING THEORY

In the theoretical framework of a random resistor network,[21] percolation is specified by considering the separation of localized donor and acceptor states in real (r_{ij}) and energy space (ε_{ij}). Each pair of states is connected by an ideal resistor with the resistance being proportional to the exponent of the corresponding percolation value ξ_{ij}, which has an upper limit ξ_C in each macroscopic system,[22] and may be expressed by

$$\xi_C \geqslant \xi_{ij} = \frac{2r_{ij}}{a} + \frac{\varepsilon_{ij}}{k_B T}, \tag{2}$$

a is a localization length which scales the dependence of ξ_{ij} upon the hopping distance. We have approximated a by the Mn ionic radii due to the lack of the exact r_{ij} dependence of ξ_{ij}.

Macroscopically, the resistivity ρ is dominated by resistors close or approximately at the percolation threshold, and

$$\rho = \rho_0 \exp(\xi_C), \tag{3}$$

where ρ_0 depends on particular physical and material properties of the system. The real space and energy separation of states compete with each other and the relative magnitudes of the two terms of ξ_C [on the right-hand side of (2)] determine whether or not hopping is constrained to nearest neighbors, and evidently at sufficiently high temperatures it always is. A simple estimate for $NiMn_2O_{4+\delta}$ shows that both terms in (2) equal at ~300 K, and VRH might occur up to this temperature in consequence. In fact the VRH-NNH transition temperature might be higher, when the r_{ij} term is clearly dominating. For this estimation the minimum distance of octahedral sites was used for r_{ij}, the ionic radius of the Mn^{3+} cation for a,[23] and the activation energy from bulk measurements[4] for ε_{ij}. The standard Holstein small polaron hopping model[24,25] in the nonadiabatic limit is applicable for $NiMn_2O_{4+\delta}$,[14] and for NNH it leads to an expression of the form

$$\rho = C_1 k_B T \exp\left(\frac{\varepsilon_3}{k_B T}\right), \tag{4}$$

where C_1 comprises several temperature independent parameters including the term $\exp(2r_C/a)$. For NNH r_{ij} reduces to the constant critical radius r_C. Several material specific constants in C_1 are not known for $NiMn_2O_{4+\delta}$ and precise quantitative analysis of R-T data is not possible by following this approach.

Electrons hop to a more remote site if the separation in energy is favorable and a lower percolation value ξ_{ij} can be achieved than for a relevant nearest-neighbor hop. The maximum energy separation of contributing states permitted by the threshold parameter ξ_C is $\varepsilon_{\max}$, and the maximum real space separation $r_{\max}$.[26] Explicit expressions for $\varepsilon_{\max}$ and $r_{\max}$ can be derived by following the celebrated variable-range hopping (VRH) model from Mott,[27] but it only applies if the DOS $g(\varepsilon_F)$ can be assumed to be constant in the energy range of interest. In a more general approach a parametrized DOS $g(\varepsilon)$ (parameters g', z) may be used,[28]

$$g(\varepsilon) = g' \varepsilon^Z, \tag{5}$$

where ε is the energy of electrons with the zero level set to Fermi level. It was assumed that the DOS vanishes at Fermi level, as a result of Coulomb interactions of electrons. Explicit expressions for $\varepsilon_{\max}$ and $r_{\max}$ for a parametrized DOS were derived following the Shklovskii and Efros (SE) model.[22] Substituting these into (3) and assuming a nonadiabatic small polaron pre-exponential factor ρ_0, leads to[28]

$$\rho = C_2 (k_B T)^{2p} \exp\left(\frac{T_0}{T}\right)^p, \tag{6}$$

where p is given by $p=(z+1)/(z+4)$ and C_2 comprises all constants. In the general case T_0 is given by

$$T_0 = \frac{1}{k_B}\left(\frac{21.2}{a^3 g'}(z+1)\right)^{1/(z+1)}. \tag{7}$$

IV. DATA ANALYSIS

For all types of $NiMn_2O_{4+\delta}$ materials R-T data were analyzed by the method described by SE,[22] which enables the index parameter p in (6) to be determined. This allows us to decide which VRH model provides the best description of the R-T data or if NNH occurs ($p=1$). p is the negative slope of a plot $\ln(W)$ vs $\ln(T)$, where W is defined as

$$W = \frac{1}{T}\frac{d(\ln \rho)}{d(T^{-1})} \approx -p\left(\frac{T_0}{T}\right)^p. \tag{8}$$

This is a powerful technique to elucidate the character of hopping motion, but it should be noted that it is a differentiation method and is therefore sensitive to scatter in the original R-T characteristics. The slope of $\ln(W)$ vs $\ln(T)$ can be regarded only as an approximation for p, because in (8) the following assumptions for NNH and VRH were made:

$$|-1| \ll \frac{T_0}{T}, \quad \text{NNH}, \tag{9}$$

$$|-2p| \ll p\left(\frac{T_0}{T}\right)^p, \quad \text{VRH}. \tag{10}$$

In order to determine the characteristic temperature T_0, data were plotted as $\ln(R/T)$ vs $1/T$ for NNH and $\ln(R/T^{2p})$ vs $1/T^p$ for VRH. A standard linear least-square fitting routine was used to obtain T_0 and p from the slopes of the relevant graphs.

V. EXPERIMENT

A. Sample preparation

Phase pure $NiMn_2O_{4+\delta}$ powder was produced by mixing and firing precursor oxides for pressing pellets and as a source for thin film deposition by EBE.[29] For screen-printing, $NiMn_2O_{4+\delta}$ powder was produced via coprecipitation of nickel manganese oxalate and subsequent firing.[30,17] Thick films of ~ 20 μm thickness were printed via a standard screen-printing process.[17] A glass phase, organic dispersing agent, organic solvents, and organic binder were added to the source powder to produce printing pastes. Films were printed on polycrystalline Al_2O_3 substrates and all organic components were decomposed after printing by thermal decomposition followed by a sintering densification process. The glass phase exhibited a low viscosity at higher temperatures and liquid phase sintering occurred, which compacted the ceramic grains by capillary action. One set of samples was prepared without glass and dispersing agent.

Thin films (~ 0.5 μm-1 μm) were deposited onto polycrystalline Al_2O_3 substrates with predigitated Pt electrodes.[30] EBE was carried out using a standard evaporation kit at pressures of $10^{-2}-10^{-3}$ Pa with a low deposition rate of 0.8 nm s^{-1}. During deposition the substrates were heated to 100 °C, and annealed after in air at 200 °C, 300 °C, 400 °C, and 500 °C for 30 min. One sample was kept in the as-deposited state. A problem with EBE was to reproduce the stoichiometry of the source powder in the films, as well as from run to run, and to ensure phase purity.[9]

B. Resistance vs temperature characterizations

For samples without predigitated electrodes, two circular Al electrodes were evaporated onto the film or pellet surfaces, and were covered with silver to prevent oxidation. Copper wires were attached with solder and the ohmic behavior of the electrodes was confirmed. The current vs voltage (I-V) characteristics of $NiMn_2O_{4+\delta}$ exhibit a nonlinear regime above a critical current (turnover), and for R-T measurements it was ensured that the I-V working point was in the linear regime. The nonlinearity is a thermal runaway effect,[31–33] resulting from self-heating due to current heat dissipation.

Low temperature regime (LTR) R-T characteristics (150 K–330 K) were measured in a standard evacuated and He gas backfilled cryostat system connected to a Keithley 617 electrometer and a temperature controller linked to two ceramic encapsulated Pt resistance thermometers. One thermometer was placed directly beneath the sample to gain optimum accuracy of sample temperature measurements. This

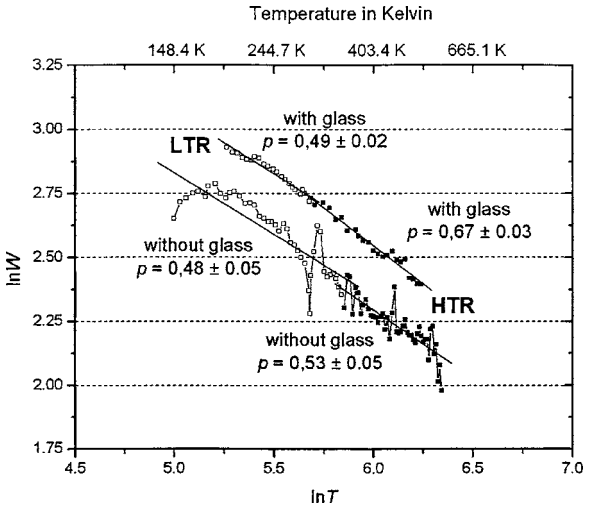

FIG. 2. ln W vs ln T plots for screen-printed films, sintered at 850 °C for 30 min, HTR and LTR, the graphs for films with glass are shifted by 0.25 up the ln W axis.

is of vital importance, because temperature fluctuations or inaccuracy in sample temperature measurements strongly influence the R-T characteristics due to the strong insulating behavior of exponential resistance dependence upon inverse temperature. Data was recorded using an automated data acquisition system, which ensured complete temperature and resistance stability, i.e., equilibrium between current heat dissipation and cooling system, before taking R-T readings. This type of steady-state measurement is believed to be more accurate and to lead to reduced scatter in the R-T curves.

For high temperature regime (HTR) measurements (300 K–570 K) samples were placed in a purpose built insulated furnace equipped with a temperature controller linked to a chromel-alumel thermocouple, which was placed directly onto the sample surface. Steady-state R-T readings were taken manually using the Keithley electrometer.

VI. RESULTS

A. Screen-printed films

Figure 2 shows ln W vs ln T plots for screen-printed films with and without glass phase. It is indicated that VRH occurred with a parabolic distribution of the DOS $g(\varepsilon)$, as p was close to 0.5. The uncertainties in p arising from the linear least-square fitting routine were reasonably low, calculated for each graph according to the method given by Taylor.[34] The right-hand side of (10) was in the range of 18.8–9.2 and at high temperatures p might contain a perceptible error. Nevertheless, the conduction mechanism was believed to be identified unambiguously and the resistivity ρ was estimated from the sample geometry and the R-T data and plotted as $\ln(\rho/T)$ vs $1/T^{0.5}$ in Fig. 3. The misalignment of LTR and HTR curves may be a result of inaccuracy in estimating the resistivity from the cross section of the conducting path in the sample and of the different contacts and thermocouples used for HTR and LTR measurements.

A parabolic distribution of the DOS had previously been confirmed by low energy STM/STS measurements on thin (~200 nm) films, sputter deposited on ⟨100⟩ oriented Si substrates and annealed at 800 °C for 1 h, which revealed DOS features consistent with upper and lower Hubbard bands (Fig. 4).[11] The parabolic parametrization of the DOS $g(\varepsilon)$ was justified in the proximity of Fermi level as can be seen in Fig. 4. The band maxima are separated by an energy interval close to the activation energy ε_3 previously determined

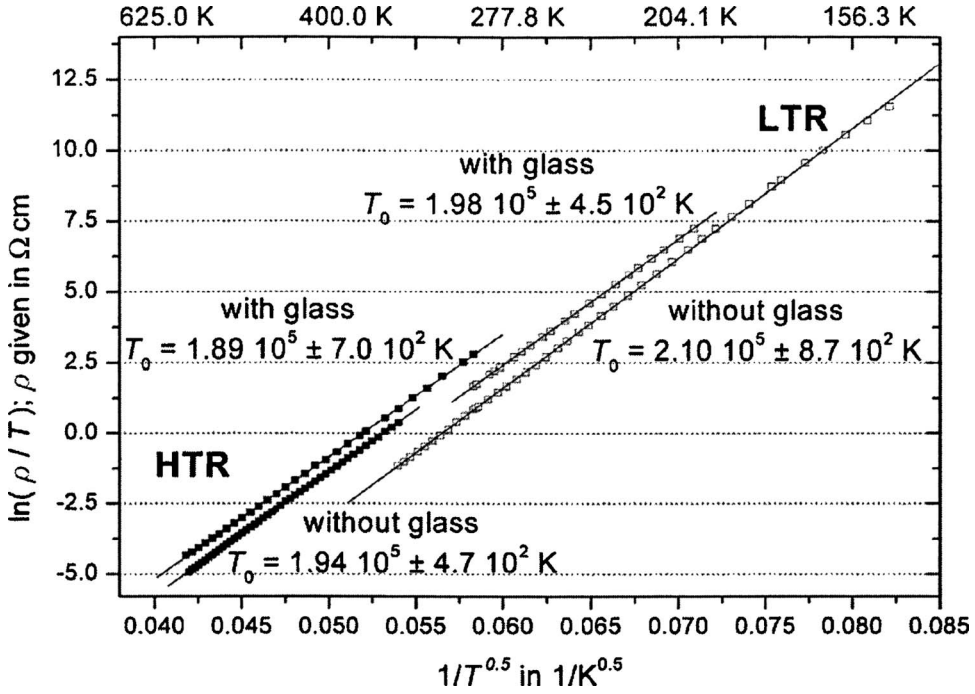

FIG. 3. $\ln(\rho/T)$ vs $1/T^{0.5}$ plots for screen-printed films with and without glass phase, sintered at 850 °C for 30 min, HTR and LTR.

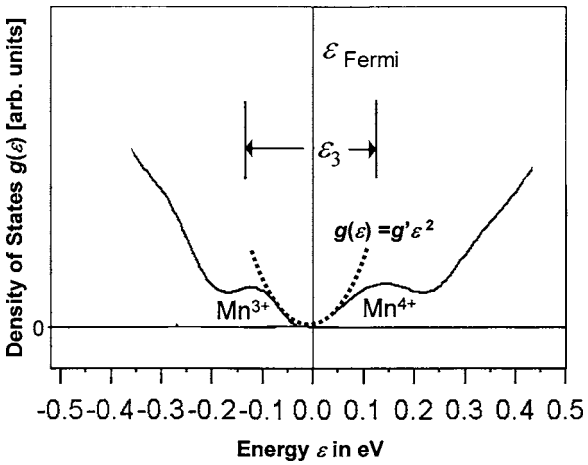

FIG. 4. Low energy STM/STS, DOS vs electron energy for a sputter deposited and 800 °C annealed film, heated to 300 °C (reproduced from Ref. 11).

from a NNH model.[4] As ε_3 contains a contribution from the polaron formation energy, electron states contributing to conduction may be well within the parabolic parametrization limits. By using the Mn^{3+}/Mn^{4+} cation radii from a hard sphere model as an estimate for a ($a \sim 0.7$ Å),[23] g' was obtained from T_0 and $g(\varepsilon)$ calculated at ±0.15 eV where the DOS shows two local maxima at the upper and lower Hubbard bands. T_0, the room temperature (20 °C) resistivity ρ_{RT}, the $g(0.15\ \text{eV})$ values, the percolation threshold ξ_C and the maximum energy and spatial separation of contributing electron states ε_{max} and r_{max} are shown in Table I; the values given are variations in the measured temperature range. The $g(0.15\ \text{eV})$ values are low compared to crystalline semiconductors such as Ge, where $g(\varepsilon)$ is in the order of $10^{22}\ \text{cm}^{-3}\ (\text{eV})^{-1}$ at the conduction band edge.[35] On the other hand, the DOS in disordered amorphous heavily H-doped silicon at low temperatures in the impurity conduction regime is in the order $10^{17}-10^{18}\ \text{cm}^{-3}\ (\text{eV})^{-1}$,[27] and the values obtained for $NiMn_2O_{4+\delta}$ are closer to the crystalline reference. The ε_{max} values of 0.48–0.91 eV are higher than the NNH activation energies ε_3 reported for $NiMn_2O_{4+\delta}$ in the literature ($\sim$0.3–0.4 eV),[4,13] possibly because a maximum energy separation requires that the spatial separation tends to 0. This is not possible in polycrystalline $NiMn_2O_{4+\delta}$ where the minimum spatial separation is the distance of octahedral sites, i.e., 3.0 Å. Another source of error may be the estimation for a.

The r_{max} values obtained are all higher than 3.0 Å at all temperatures, and with the model used only at $\sim$2600 K would r_{max} be close to 3.0 Å and a transition to NNH be expected. Alternatively, the transition from VRH to NNH may be assumed to occur if r_{max} drops below the distance to the next nearest neighbor, i.e., 5.14 Å, and the transition would be at $\sim$850 K.

B. Pressed pellets

ln W vs ln T plots for pellets sintered at different temperatures are given in Fig. 5. The factors p were all higher than 0.5, with a mean value of 0.65 and a standard deviation σ of 0.04. The approximation in (10) was not critical, as the right-hand side was in the range from 19.86 to 12.79. The p value of 0.65 was interpreted as a deviation of the DOS from a strict parabolic shape to a z value of $\sim$4.6. This dependency can be explained by a depletion of electron states near Fermi level and a steep increase near the Mn^{3+}/Mn^{4+} band centers.

TABLE I. Characteristic temperature T_0 in K from $\ln(R/T)$ vs $1/T^{0.5}$ plots, ρ_{RT} in Ω cm, $g(0.15\ \text{eV})$ in $\text{eV}^{-1}\ \text{cm}^{-3}$, ε_{max}, r_{max}, and ξ_C for screen-printed films with and without glass phase.

	With glass phase		Without glass phase	
	LTR	HTR	LTR	HTR
Temperature range in K	193–294	294–573	148–339	338–573
T_0 in Kelvin	1.98×10^5 $\pm5\times10^2$	1.89×10^5 $\pm7\times10^2$	2.10×10^5 $\pm9\times10^2$	1.94×10^5 $\pm5\times10^2$
ρ_{RT} in Ω cm	1.6×10^3	5.0×10^3	0.86×10^3	(3.5×10^3)
$g(0.15\ \text{eV})$ in $\text{eV}^{-1}\ \text{cm}^{-3}$	8.5×10^{20}	9.6×10^{20}	7×10^{20}	8.9×10^{20}
ε_{max} in eV increase T	0.53–0.66	0.64–0.90	0.48–0.73	0.70–0.91
r_{max} in Å increase T	11.2–9.1	8.9–6.4	13.2–8.7	8.4–6.4
ξ_C increase T	31.9–25.9	25.4–18.2	37.7–24.9	24.0–18.4

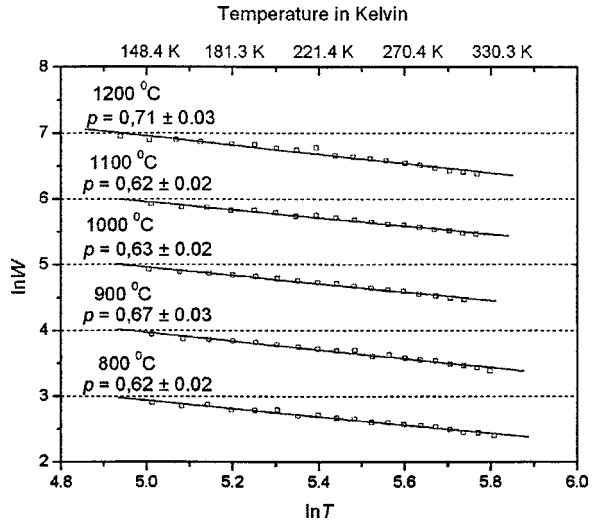

FIG. 5. ln W vs ln T plots for pressed pellets, sintered at different temperatures for 24 hours and annealed at 800 °C for 40 hours, LTR, the graphs for 900 °C–1200 °C are shifted up the ln W axis by 1 each.

It is suggested that this distribution indicates a higher level of disorder in the material, which leads to a narrower electronic bandwidth associated with stronger localization effects. Here, the most obvious explanation for such differences in disorder is the grain structure, which is fundamentally different in thick films and pellets. In pellets grains have random shapes and are arranged in a brick layer fashion with negligible porosity,[36] whereas in screen-printed films the grains show a spherical shape and are arranged in a closed packed formation with weaker intergrain contact exhibiting considerable porosity.[17] Again, the difference in grain structure is a result of different production processes, pellets were pressed and sintered at high temperature for up to 50 hours, thick films were printed and sintered at lower temperatures over a minimized time period of 30 min.

The pellet ρ-T data were plotted as $\ln(\rho/T^{1.3})$ vs $1/T^{0.65}$, the corresponding T_0, ρ_{RT}, $g(0.15\ \mathrm{eV})$, $\varepsilon_{\max}$, $r_{\max}$, and ξ_C values are given in Table II, The p values showed good consistency, indicating that the hopping mechanism was not altered qualitatively by the different sintering temperatures applied. The T_0 and $g(0.15\ \mathrm{eV})$ values showed a decrease compared to the screen-printed samples, but again were found to be independent on sintering temperature. $\varepsilon_{\max}$, $r_{\max}$, and ξ_C seemed to be not correlated to the sintering temperature either.

C. Electron-beam evaporated films

ln W vs ln T plots in the HTR for films in the as-deposited and postdeposition annealed state are shown in Fig. 6. Conduction was probably by NNH as p tended to 1 except when annealed at 200 °C and 400 °C, where lower values of $p=0.63$ and 0.69 are displayed. The differences in p for 200 °C and 400 °C annealed samples could be due to a high level of scatter in the original R-T data, which reflects the fact that the curves are of differentiated data and therefore particularly susceptible to noise. Such high noise level might arise out of the fact that the films were very thin ($<1\ \mu$m) and exhibited high resistances up to $10^9\ \Omega$. Another matter of concern was the approximation made in (9). T_0/T was in the range of 17.5–10.9 and especially at higher temperatures the p values might contain a perceptible error. Still, it was decided to describe conduction by NNH and the R-T data were plotted on the $\ln(R/T)$ vs $1/T$ axes shown in Fig. 7.

The possible occurrence of NNH in thin films is again interpreted as a result of increased disorder. Thin films exhibited poor crystallinity in the as-deposited state, which only slightly improved upon annealing at a comparatively low heat exposure up to 400 °C for 30 min.[9] Here, the dis-

TABLE II. Characteristic temperature T_0 in K from $\ln(R/T^{1.3})$ vs $1/T^{0.65}$ plots, ρ_{RT} in Ω cm, $g(0.15\ \mathrm{eV})$ in $\mathrm{eV}^{-1}\ \mathrm{cm}^{-3}$, $\varepsilon_{\max}$, $r_{\max}$, and ξ_C for pellets sintered at different temperatures, LTR.

	800 °C	900 °C	1000 °C	1100 °C	1200 °C
Temperature range in K	150–333	150–330	149–311	150–319	140–320
T_0 in Kelvin	3.05×10^4 $\pm9\times10^2$	3.12×10^4 $\pm1\times10^3$	3.13×10^4 $\pm1.1\times10^3$	3.13×10^4 $\pm1\times10^3$	3.04×10^4 $\pm9\times10^2$
ρ_{RT} in Ω cm	1.5×10^4	1.5×10^4	7.0×10^3	6.63×10^3	3.7×10^3
$g(0.15\ \mathrm{eV})$ in $\mathrm{eV}^{-1}\ \mathrm{cm}^{-3}$	2.5×10^{20}	2.2×10^{20}	2.2×10^{20}	2.2×10^{20}	2.5×10^{20}
$\varepsilon_{\max}$ in eV increase T	0.41–0.54	0.42–0.55	0.42–0.54	0.42–0.54	0.40–0.53
$r_{\max}$ in Å increase T	11.1–6.6	11.2–6.7	11.3–7.0	11.3–6.9	11.6–6.8
ξ_C increase T	31.6–18.8	32.1–19.2	32.3–20.1	32.2–19.7	33.1–19.3

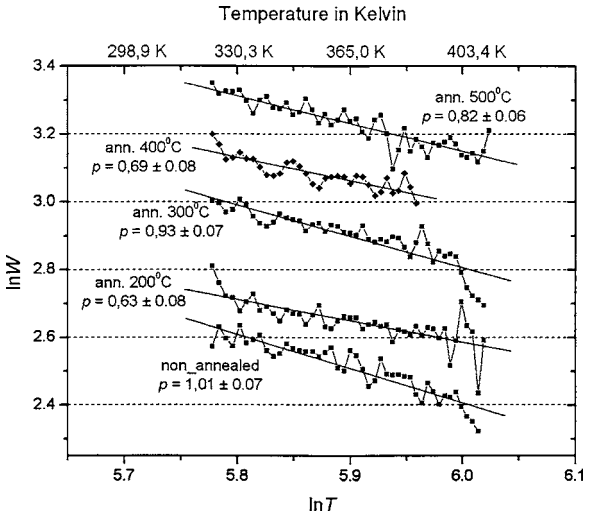

FIG. 6. ln W vs ln T graphs for EBE films, annealed at different temperatures for 30 min, HTR, the annealed graphs are shifted up the ln W axis by 0.1, 0.3, 0.5, 0.8.

order may lead to such strong electron localization that the parametrization of Eq. (5) is no longer valid. Mn^{3+} and Mn^{4+} bands may then be separated by an energy gap, and a small bandwidth associated with strong localization rules out the competition between energy and real space separation of localized states, required for VRH.

The characteristic temperatures and activation energies ($\varepsilon_3 = k_B T_0$) are given in Table III. T_0 and ε_3 in the films are slightly higher than the values previously reported for polycrystalline bulk material. For measurements between 385 K–550 K Brabers and Terhell gave $\varepsilon_3 = 0.37$ eV,[4] and Feltz *et al.* gave $T_0 = 3.8 \times 10^3$ K ($\varepsilon_3 = 0.33$ eV) for 273 K–343 K.[13] The change of activation energy ε_3 with annealing temperature is illustrated in the inset of Fig. 7. In addition, the pre-exponential factor C_1 from Eq. (4) was plotted as $1/C_1$ vs annealing temperature, determined from the intercepts of the linear least-squares fit to the R-T data. As expected $1/C_1$ followed a similar trend as ε_3. According to small polaron hopping theory C_1 is proportional to $1/\varepsilon_{ij}$ (corresponding to ε_3 in NNH).[22]

VII. DISCUSSION AND CONCLUSIONS

Different types of electron hopping were detected in different kinds of $NiMn_2O_{4+\delta}$ materials, NNH in thin EBE films, and VRH in screen-printed films and pressed pellets. It is argued that differences in the exponent p of the power law relationship of resistance and temperature can be associated with different levels of disorder in the material as a result of variations in microstructure. Thin EBE films exhibited a high level of scatter in the R-T data, probably due to high resistances up to $10^9/\Omega$, which resulted in difficulties in the p-factor analysis. In contrast, the identification of VRH in pellets and thick films was very clear, the resistances were lower here and the production processes were probably more controlled.

The VRH model in screen-printed films and pellets is still valid at higher temperatures, although it has been developed

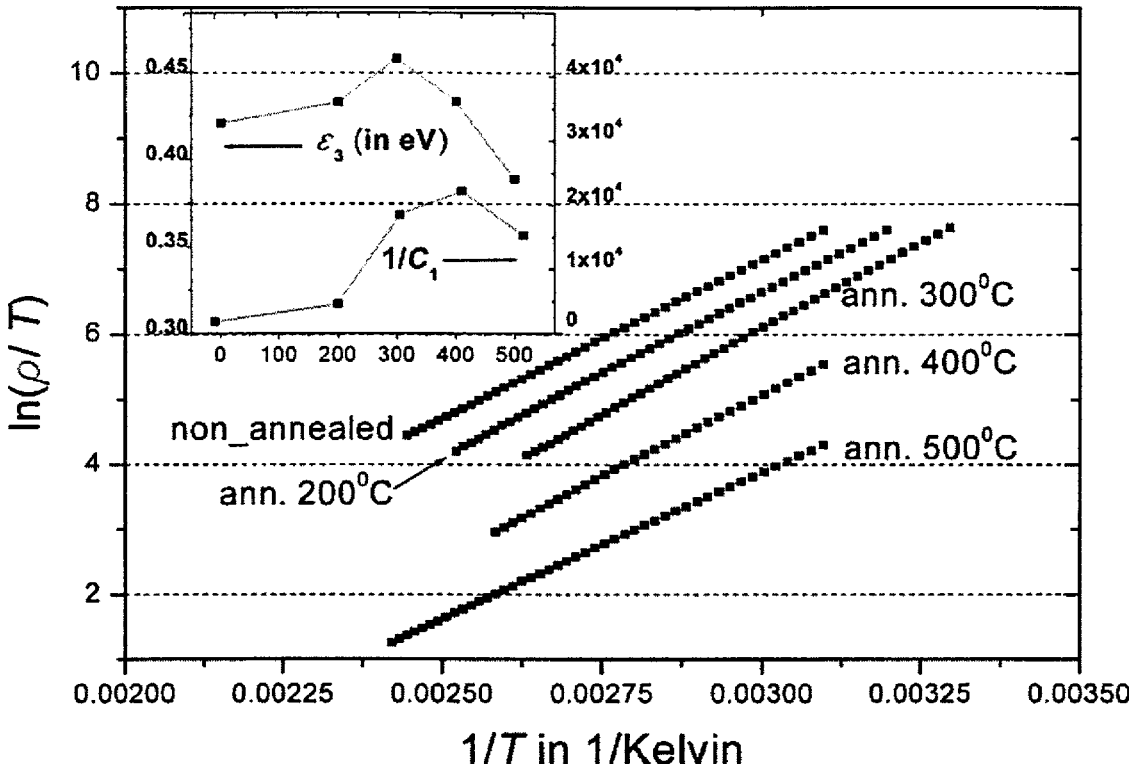

FIG. 7. ln(R/T) vs $1/T$ for EBE films, annealed at different temperatures for 30 min, HTR; the graphs for the films annealed at 200 °C and 300 °C are shifted by +0.0001 and +0.0002 on the $1/T$ axis. Inset, pre-exponential factor $1/C_1$ and activation energy ε_3 vs annealing temperature.

TABLE III. Characteristic temperature T_0 in K and activation energy ε_3 in eV from $\ln(R/T)$ vs $1/T$ plots for EBE films, annealed at different temperatures, HTR.

	Nonannealed	200 °C	300 °C	400 °C	500 °C
Temperature range in K	323–409	323–413	323–411	323–413	323–413
T_0 in K	$4.9\times10^3\pm4$	$5.0\times10^3\pm10$	$5.3\times10^3\pm10$	$5.0\times10^3\pm10$	$4.5\times10^3\pm5$
ε_3 in eV	0.42 eV	0.43 eV	0.46 eV	0.43 eV	0.39 eV

originally to explain the low temperature impurity conduction in (doped) CS. The r_{ij} term in expression (2) must be sufficiently small even at higher temperatures, which would require a small distance between acceptor and donor. The Mn^{3+} and Mn^{4+} concentration in $NiMn_2O_{4+\delta}$ is some orders of magnitude higher than any impurity concentration in crystalline or amorphous material and r_{ij} would be indeed comparably small in consequence. This is consistent with the findings in Sec. VI A, where it was suggested that the DOS $g(\varepsilon)$ in thick films is higher than in a typical impurity conduction regime. Generally, the use of VRH models in manganese oxides is quite widely accepted.[37–40]

A problem with the application of a VRH model to $NiMn_2O_{4+\delta}$ is the fact that the scaling factor a needs to be estimated to calculate $g(\varepsilon)$, or vice versa. A theoretical study would be useful to calculate a in spinel manganates; the calculation or measurement of both, a and $g(\varepsilon)$, would allow even better in-depth analysis. In this context it is also interesting to note that NNH and VRH theories are not compatible with each other. NNH is not the high temperature (or low concentration, or high electron localization) limit of VRH and, to our knowledge, there is no comprehensive theory available to describe the behavior of a system in an intermediate regime between NNH and VRH.

In conclusion, it was shown on the example of $NiMn_2O_{4+\delta}$ that the concept of localized polaron hopping in the impurity conduction regime in doped semiconductors may also be valid in spinel manganese oxides at all temperatures where electrons show a high degree of localization and transport is by small polaron hopping. In $NiMn_2O_{4+\delta}$ electron-beam evaporated thin films conduction was by NNH. Pressed pellets and screen-printed films showed VRH conduction with an approximately parabolic distribution of the DOS around Fermi level, and the R-T data seemed to be more reliable.

It is suggested that screen-printed films may be an excellent solution for various applications of spinel manganates as thermistor material where the advantages of films compared to bulk could be fully exploited. Thin films exhibit high resistances and vapor deposition involves more technological challenges than direct printing techniques. Screen printing of spinel manganates may well be suitable for commercial low cost volume production in microelectronic industry.

ACKNOWLEDGMENTS

The authors wish to thank A. Roosen and A. Stiegelschmitt for guidance developing screen-printing procedures. Thanks to Z. Klusek and P. K. Datta for carrying out STM/STS measurements, thanks to J. Evans for allowing use of the XRD facilities. Thanks for valuable discussions with A. Feltz, G. Döhler, I. Terry, G. Ashcroft, and T. Hashemi. One of the authors (A.B.) would like to acknowledge financial support from the Overseas Research Scholarship (ORS) scheme and the University of Durham.

*Author to whom correspondence should be addressed. Present address: University of Cambridge, Department of Materials Science and Metallurgy, Pembroke Street, Cambridge CB2 3QZ, United Kingdom. Electronic address: rs441@cam.ac.uk

[1] N. Tsuda, K. Nasu, A. Fujimori, and K. Siratori, in *Electronic Conduction in Oxides*, Solid-State Sciences, edited by M. Cardona, P. Fulde, K. von Klitzing, R. Merlin, H. J. Queisser, and H. Störmer (Springer, Berlin, 2002).

[2] E. D. Macklen, *Thermistors* (Electrochemical Publications, Glasgow, 1979).

[3] A. Feltz and J. Töpfer, Z. Anorg. Allg. Chem. **576**, 71 (1989).

[4] V. A. M. Brabers and J. C. J. M. Terhell, Phys. Status Solidi A **69**, 325 (1982).

[5] J. L. Baudour, F. Bouree, M. A. Fremy, R. Legros, A. Rousset, and B. Gilot, Physica B **180-181**, 97 (1992).

[6] J. Töpfer, A. Feltz, D. Gräf, B. Hackl, L. Raupach, and P. Weissbrodt, Phys. Status Solidi A **134**, 405 (1992).

[7] S. Asbrink, A. Waskowska, M. Drozd, and E. Talik, J. Phys. Chem. Solids **58**, 725 (1997).

[8] W. D. Kingery, H. K. Bowen, and D. R. Uhlmann, *Introduction to Ceramics* (Wiley, New York, 1960).

[9] R. Schmidt, Ph.D. thesis, University of Durham, 2003.

[10] G. Kotliar and D. Vollhardt, Phys. Today **57**, 53 (2004).

[11] R. Schmidt, A. Basu, A. W. Brinkman, Z. Klusek, and P. K. Datta, Appl. Phys. Lett. **86**, 073501 (2005).

[12] J. A. Becker, C. B. Green, and G. L. Pearson, Bell Syst. Tech. J. **26**, 170 (1947).

[13] A. Feltz, J. Töpfer, and F. Schirrmeister, J. Eur. Ceram. Soc. **9**, 187 (1992).

[14] S. Fritsch, J. Sarrias, M. Brieu, J. J. Couderc, J. L. Baudour, E. Snoeck, and A. Rousset, Solid State Ionics **109**, 229 (1998).

[15] A. H. Feingold, R. L. Wahlers, P. Amstutz, H. C. S. J. Stein, and

J. Mazzochette, Microwave J. **2000**, 90 (2000).
[16] J. Zhong and H. H. Bau, Am. Ceram. Soc. Bull. **80**, 39 (2001).
[17] R. Schmidt, A. Stiegelschmitt, A. Roosen, and A. W. Brinkman, J. Eur. Ceram. Soc. **23**, 1549 (2003).
[18] M. Parlak, T. Hashemi, M. J. Hogan, and A. W. Brinkman, J. Mater. Sci. Lett. **17**, 1995 (1998).
[19] A. Basu, Ph.D. thesis, University of Durham, 2002.
[20] R. Schmidt, A. Basu, and A. W. Brinkman, J. Eur. Ceram. Soc. **24**, 1233 (2004).
[21] A. Miller and E. Abrahams, Phys. Rev. **120**, 745 (1960).
[22] B. I. Shklovskii and A. L. Efros, in *Electronic Properties of Doped Semiconductors*, Solid State Sciences 45, edited by M. Cardona, P. Fulde, and H. J. Queisser (Springer-Verlag, Berlin, 1984).
[23] H. S. C. O'Neill and A. Navrotsky, Am. Mineral. **68**, 181 (1983).
[24] T. Holstein, Ann. Phys. (N.Y.) **8**, 343 (1959).
[25] I. G. Austin and N. F. Mott, Adv. Phys. **18**, 41 (1969).
[26] F. R. Allen and C. J. Adkins, Philos. Mag. **26**, 1027 (1972).
[27] N. F. Mott, *Conduction in Non-Crystalline Materials* (Clarendon, Oxford Science Publications, Oxford, 1993).
[28] R. Mansfield, in *Hopping Transport in Solids*, edited by M. Pollak and B. Shklovskii (Elsevier Science, Amsterdam, 1991), p. 349.
[29] A. P. B. Sinha, N. R. Sanjana, and A. B. Biswas, Acta Crystallogr. **10**, 439 (1957).
[30] R. Schmidt and A. W. Brinkman, Int. J. Inorg. Mater. **3**, 1215 (2001).
[31] F. J. Hyde, J. Electron. **1**, 303 (1955).
[32] R. E. Burgess, J. Electron. **1**, 297 (1955).
[33] I. Brunets, O. Mrooz, O. Shpotyuk, and H. Altenburg, *Proceedings of the 24th International Conference on Microelectronics (MIEL, 2004)* (Nis, Serbia and Montenegro, 2004), Vol. 2.
[34] J. R. Taylor, in *An Introduction to Error Analysis*, A Series of Books in Physics, edited by E. D. Commins (University Science Books, Mill Valley, 1982), p. 159.
[35] H. Ibach and H. Lüth, *Festkörperphysik* (Springer Verlag, Berlin, 1995), p. 145.
[36] R. Schmidt, A. Basu, A. W. Brinkman, T. P. A. Hase, Z. Klusek, S. Pierzgalski, and P. K. Datta, Surf. Sci. (to be published).
[37] J. M. D. Coey, M. Viret, and L. Ranno, Phys. Rev. Lett. **75**, 3910 (1995).
[38] R. Laiho, K. G. Lisunov, E. Laehderanta, V. N. Stamov, and V. S. Zakhvalinskii, J. Phys.: Condens. Matter **13**, 1233 (2001).
[39] Y. Sun, X. Xu, and Y. Zhang, J. Phys.: Condens. Matter **12**, 10475 (2000).
[40] S. Baliga and A. L. Jain, Mater. Lett. **11**, 226 (1991).